First cross-section measurements of the reactions ^{107,109}Ag$(p,\gamma)^{108,110}$Cd at energies relevant to the p process

A. Khaliel,* T. J. Mertzimekis,† E.-M. Asimakopoulou, A. Kanellakopoulos, V. Lagaki, A. Psaltis, I. Psyrra, and E. Mavrommatis
Department of Physics, University of Athens, Zografou Campus, GR-15784 Athens, Greece
(Received 26 July 2017; published 28 September 2017)

Background: One of the primary objectives of the field of Nuclear Astrophysics is the study of the elemental and isotopic abundances in the universe. Although significant progress has been made in understanding the mechanisms behind the production of a large number of nuclides in the isotopic chart, there are still many open questions regarding a number of neutron-deficient nuclei, the p nuclei. To that end, experimentally deduced nuclear reaction cross sections can provide invaluable input to astrophysical models.
Purpose: The reactions ^{107,109}Ag$(p,\gamma)^{108,110}$Cd have been studied at energies inside the astrophysically relevant energy window in an attempt to provide experimental data required for the testing of reaction-rate predictions in terms of the statistical model of Hauser-Feshbach around the p nucleus ^{108}Cd.
Methods: The experiments were performed with in-beam γ-ray spectroscopy with proton beams accelerated by the Tandem Van de Graaff Accelerator at NCSR "Demokritos" impinging a target of natural silver. A set of high-purity germanium detectors was employed to record the emitted radiation.
Results: A first set of total cross-section measurements in radiative proton-capture reactions involving ^{107,109}Ag, producing the p-nucleus ^{108}Cd, inside the astrophysically relevant energy window is reported. The experimental results are compared to theoretical calculations, using TALYS. An overall good agreement between the data and the theoretical calculations has been found.
Conclusions: The results reported in this work add new information to the relatively unexplored p process. The present measurements can serve as a reference point in understanding the nuclear parameters in the related astrophysical environments and for future theoretical modeling and experimental works.

DOI: 10.1103/PhysRevC.96.035806

I. INTRODUCTION

The bulk of heavier elements can be produced by two distinct neutron-capture processes, known as the s and r processes [1,2]. Despite the success of these processes in describing the production of the majority of the known isotopes in the nuclear landscape, they fail to produce approximately 35 stable neutron-deficient nuclei between ^{74}Se and ^{196}Hg [3]. Consequently, another process was suggested to explain the origin of these nuclei [1], called the p process. The p process practically involves every mechanism able to synthesize a p nucleus. The p nuclei [4,5] are those isotopes that are characterized by a mass number $A > 74$, lie on the neutron-deficient side of the valley of stability, and are bypassed by the neutron-capture chains (s and r processes). The nuclei synthesized by the p process, despite being stable, are remarkably less abundant than the ones produced by s and r processes, typically in the range of 10^{-3} to 10^{-1} [6,7].

Several mechanisms have been proposed to explain the production of the p nuclei in various astrophysical environments (see, e.g., Ref. [8]). The dominant theory suggests that massive stars can produce p nuclei through photodisintegration of pre-existing intermediate and heavy nuclei in type II supernovae (SN) [4,9–12] or type Ia SN [13]. This procedure is known as the "γ process" and the most explored astrophysical site is the explosive O/Ne burning layers of core-collapse SN. Photodisintegrations can create p nuclei, either by destructing their neutron-richer isotopes through sequential (γ,n) reactions (which are the predominant photodisintegration processes for most stable nuclei) or by flows from heavier elements via (γ,p) and (γ,α) reactions and β decays. Additional mechanisms may be responsible for the p nucleosynthesis, such as the rp process [14,15], the pn process [16], and the νp process [17], not necessarily occurring in SN astrophysical environments.

One of the most important factors that needs to be understood in detail is the reaction flows to, from, and around p nuclei. Reaction flows depend critically on the nuclear cross sections of the reactions taking place. To obtain a clear view of the general picture, a complex web of interwoven nuclear reactions has to be studied and detailed descriptions of each particular mechanism driving the participating reactions need to be achieved. Reaction cross-section measurements that are of specific interest include proton- and neutron-induced reactions on stable as well as on neutron-rich and neutron-deficient nuclei up to a few MeV [18]. Especially for the γ process, cross-section measurements of proton-capture reactions, as well as of their inverse (γ,p), which are related through the detailed balance theorem, are equally important for the study of the p process.

In this rather general framework, the study of the p nucleus ^{108}Cd is of special astrophysical interest because it is characterized by a relatively small abundance [6,7], while its predicted solar-system abundance is found to be significantly smaller than the observed one [10].

*achalil@phys.uoa.gr
†tmertzi@phys.uoa.gr

The present work is focused on the reactions ^{107,109}Ag$(p,\gamma)^{108,110}$Cd. The ^{107,109}Ag$(p,n)^{107,109}$Cd reactions for proton energies between 2.0 and 6.7 MeV have been studied in Ref. [19] along with the elastic scattering in the same energy regime. The measured (p,n) cross sections have been compared with previous results by Johnson *et al.* [20]. In addition, production cross sections of ^{107}Cd by proton-induced reactions on $^{\text{nat}}$Ag in the energy range from a threshold value of 2.22 MeV up to 40 MeV have been reported in Ref. [21].

The experimental investigations of the reactions ^{107,109}Ag$(p,\gamma)^{108,110}$Cd reported in this work have been conducted with the in-beam γ-ray spectroscopy technique [22–27] (see experimental details in Sec. II). In the recent past, similar studies in neighboring nuclei have used the activation technique [28–36] and the $4\pi\gamma$-summing technique [25,37–40]. The latter, together with a novel technique using a storage ring which has been introduced recently [41], offers opportunities for reaction measurements on unstable nuclei.

Cross sections of proton-capture radiative reactions can be estimated theoretically, using the statistical Hauser-Feshbach (HF) model [42]. Under certain conditions, this model involves three important physical quantities as inputs to calculate the cross section, i.e., the Optical Model Potential (OMP), the Nuclear Level Density (NLD), and the γ-ray Strength Function (γSF). In Sec. III, various combinations of models for these quantities have been employed in a set of HF calculations, using the TALYS [43] code. Both experimental and theoretical results are discussed in Sec. IV.

II. EXPERIMENTAL DETAILS

A. Beams

The experimental study of the ^{107,109}Ag$(p,\gamma)^{108,110}$Cd reactions was carried out with proton beams delivered by the Tandem Van de Graaff Accelerator at NCSR "Demokritos". Three proton-beam energies 2.2, 3.5, and 4 MeV were used. These energies are nicely located inside the astrophysically relevant energy window (*Gamow*) which was found to be 1.6 MeV $\leqslant E_p \leqslant$ 4.7 MeV for the present case. This energy window corresponds to temperatures inside the range $1.7 \leqslant T_9 \leqslant 3.3$ ($T_9 \equiv 10^9$ K), which is the typical temperature range of the O/Ne shell of a type II core-collapse supernova [4].

B. Target

A target of natural silver (51.839% ^{107}Ag, 48.161% ^{109}Ag [44]) has been used for this particular experiment. The target thickness ξ was measured before and after the experiment [45] using the Rutherford backscattering technique [46] and was found equal to $\xi = (458 \pm 33)$ μg cm^{-2}.

The target was turned by 30° with respect to the beam so as to avoid having any of the detectors (particularly the one placed at 90°, read below for details) masked by the target aluminum frame, thus resulting in an effective thickness of

$$\xi_{\text{eff}} = \frac{\xi}{\cos 30^\circ} = (529 \pm 38)\ \mu\text{g cm}^{-2}. \quad (1)$$

The energy loss of the beam in the $^{\text{nat}}$Ag target was calculated using SRIM 2013 [47], resulting in an average value ΔE in the range 32–22 keV for the respective proton energy range $E_p = 2.2$–4 MeV in the laboratory frame. For targets with a relatively small thickness (≈500 μg cm^{-2}), it is reasonable to assume that the beam reacts with the target with an effective energy:

$$E_{\text{eff}} = E_p - \frac{\Delta E}{2}. \quad (2)$$

The beams were stopped by a thick backing behind the silver target, consisting of gold (Au) and tantalum (Ta) layers with minor impurities of ^{19}F, having sufficient thickness to ensure a reliable and accurate charge collection. For the same reason a suppression voltage of −300 V was applied upstream on the beam line. The target and backing were altogether mounted on an electrically isolated aluminum heat sink that was kept cool during the experiment by pumping air externally.

The γ rays emitted during reactions of the beam with the backing materials were identified in the spectra to ensure there was no overlapping with the γ rays of interest, i.e., those emitted during reactions of the beam and the $^{\text{nat}}$Ag target. In addition, a dedicated beam run with just the backing confirmed that there were no γ rays overlapping with the transitions of interest.

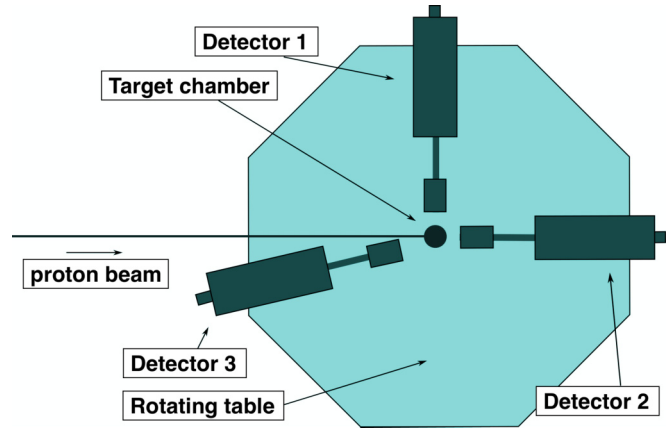

FIG. 1. A schematic representation of the experimental apparatus with the HPGe detectors and the target chamber.

C. Detection apparatus

The emitted γ rays were detected by three high-purity germanium (HPGe) detectors of 100% relative efficiency. The detectors were placed at 0°, 90°, and 165° and at respective distances of 30, 20, and 20 cm from the target (Fig. 1). All detectors were calibrated with a ^{152}Eu point-like source placed in the target's position, before and after the experiment. Absolute efficiency curves were carefully deduced for each detector from these data sets. No gain shifts were observed.

At each angle, two different 4k-long spectra per detector were recorded by splitting the preamplified signal into two amplifiers having different gain settings ("low" and "high" gain) and feeding each amplified signal to a dedicated analog-to-digital converter unit. The low-gain spectrum included γ rays with energies up to about 18 MeV and was used solely to detect the primary transition γ_0, from the entry state to the

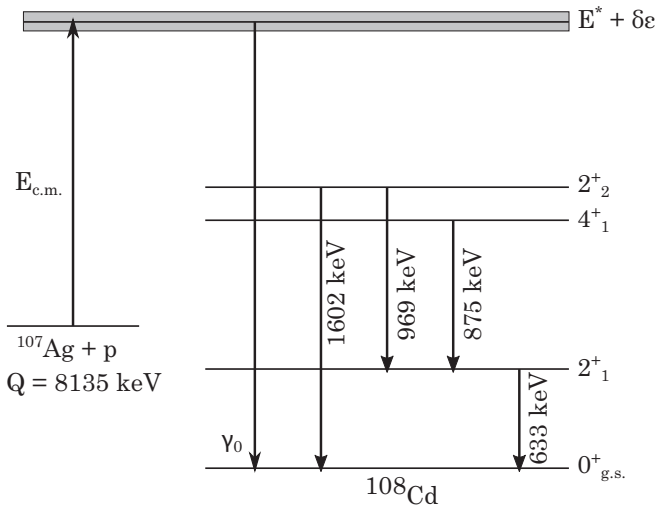

FIG. 2. A partial level scheme showing the measured transitions feeding the ground state of the produced nucleus from the reaction ^{107}Ag$(p,\gamma)^{108}$Cd [48]. The broadening of the entry state due to energy loss of the beam inside the target can be found by transforming Eq. (2) in the center-of-mass frame and is represented with $\delta\epsilon$.

ground state of the produced nucleus (Fig. 2). The high-gain spectrum focused on γ rays up to 4 MeV. The relevant part of a typical "high-gain" spectrum is shown in Fig. 3, along with the part of our interest of the respective low-gain, showing the occurrence of the primary transition γ_0 and its corresponding escape peak (EP).

III. ANALYSIS AND RESULTS

The total cross section σ_T of each reaction can be deduced by measuring the intensity of every photopeak feeding directly the ground state of the produced nucleus. The absolute yield of a transition i can be calculated by

$$Y_i = \frac{N_i(\theta_j)}{N_p \epsilon(\theta_j)}, \tag{3}$$

where, at a measuring angle θ_j, $N_i(\theta_j)$ is the dead-time-corrected intensity of a photopeak of interest, $\epsilon(\theta_j)$ is the absolute efficiency of the detector, and N_p is the number of incident protons on the target. Once the intensity N_i is measured the integral yield Y_i can be deduced. Then, by summing over all transitions i, the total absolute yield Y_{tot} can be found:

$$Y_{\text{tot}} = \sum_i^n Y_i, \tag{4}$$

where n is the total number of γ transitions feeding directly the ground state of the produced nucleus. The total number of target nuclei per unit area is

$$N_n = \frac{\xi_{\text{eff}} N_A}{M_t}. \tag{5}$$

The total cross section can now be evaluated from

$$\sigma_T = \frac{M_t}{N_A \xi_{\text{eff}}} Y_{\text{tot}}, \tag{6}$$

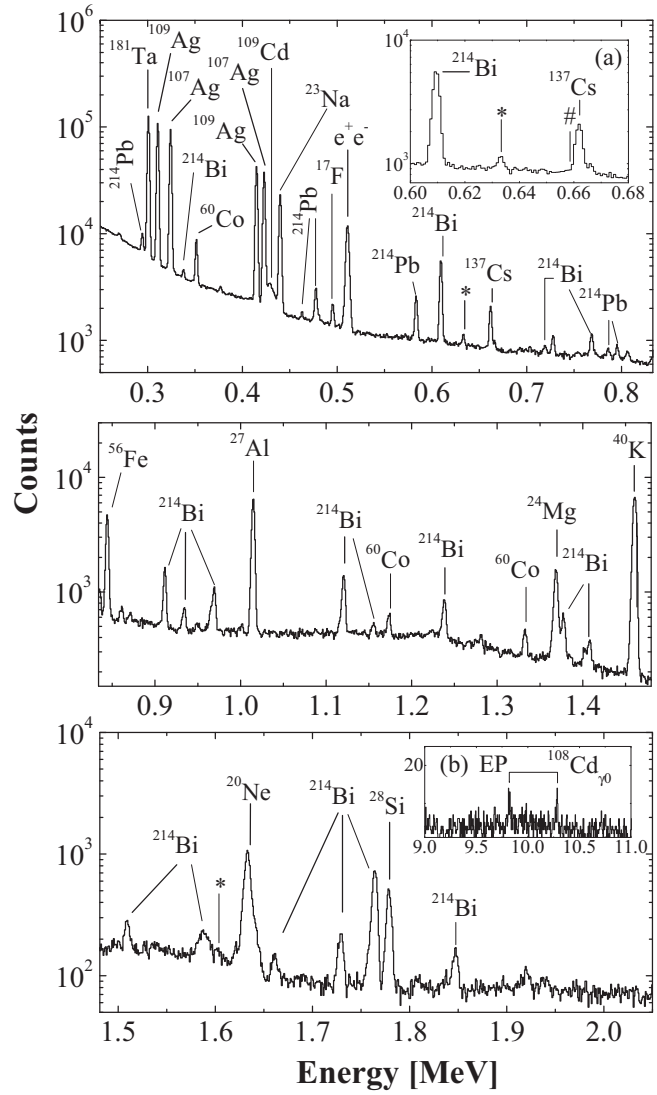

FIG. 3. Consecutive parts of a typical high-gain spectrum of the studied reactions at a proton beam energy of 2.2 MeV and an angle of 90°. Photopeaks of interest resulting from the reaction ^{107}Ag$(p,\gamma)^{108}$Cd are marked with an asterisk (∗), while those from the reaction ^{109}Ag$(p,\gamma)^{110}$Cd are marked with a hash (#). In inset (a) a more detailed view of the area of our interest is presented. The peak of ^{214}Bi is from the natural background, while the ones from ^{137}Cs and ^{60}Co originate from calibration sources placed rather far from the apparatus and used to check on gain shifts during the runs. In inset (b), the part of the respective low-gain spectrum with the ^{108}Cd γ_0 and its respective escape peak is shown. The primary transition for ^{110}Cd was not observed.

where M_t is the atomic mass of the target (in amu), N_A is Avogadro's constant, and ξ_{eff} is the effective thickness of the target [Eq. (1)].

Another useful quantity used in nuclear astrophysics is the *astrophysical S factor*, defined by the relation

$$S(E) = E\sigma(E)\exp(2\pi\eta), \tag{7}$$

where η is the Sommerfeld parameter. The astrophysical S factor varies more smoothly with energy compared to the

TABLE I. Cross sections and S factors of the reaction ^{107}Ag$(p,\gamma)^{108}$Cd vs energy. E_p(lab) is the proton beam energy in the laboratory system, $E_{\rm eff}$(lab, c.m.) is the proton beam energy corrected for energy loss in the target [Eq. (2)] in the (lab, center-of-mass) system, respectively.

E_p(lab) (keV)	$E_{\rm eff}$(lab) (keV)	$E_{\rm eff}$(c.m.) (keV)	σ (μb)	S factor (10^7 MeV b)
4000	3989	3952	103(10)	0.58(6)
3500	3488	3455	33(3)	0.82(8)
2200	2184	2164	3.6(3)	41(4)

cross section and allows for extrapolation to experimentally inaccessible energies.

A. The reaction ^{107}Ag$(p,\gamma)^{108}$Cd

For the case of ^{107}Ag$(p,\gamma)^{108}$Cd, the two lowest transitions to the ground state [48], $2_1^+ \rightarrow 0_{\rm gs}^+$ ($E_\gamma = 633$ keV) and $2_2^+ \rightarrow 0_{\rm gs}^+$ ($E_\gamma = 1602$ keV), as well as the primary transition γ_0 from the entry state to the ground state, were observed. In Fig. 3 the corresponding photopeaks from these transitions are shown for proton-beam energy equal to 2.2 MeV (lab) and the detector at 90°.

The reaction yield was determined for each detector angle after carefully measuring the photopeaks of interest, as described in the beginning of this section. No significant angular dependence was observed.

The final total cross section and the corresponding S factor values for each beam energy are shown in Table I. Quoted errors have been deduced from the statistical error arising from photopeak integration, the aggregated uncertainties of the detector absolute efficiencies, the uncertainty of the charge collected on the target (5%), and the uncertainty of the target's thickness [see Eq. (1)].

B. The reaction ^{109}Ag$(p,\gamma)^{110}$Cd

Experimental data for the reaction ^{109}Ag$(p,\gamma)^{110}$Cd suffered low statistics, mainly due to the inherently very low cross section of the reaction, in particular at 2.2 MeV. However, for the sake of completeness, extractions of total cross sections from the data were attempted. Results were obtained for all beam energies.

In this case, γ rays from the $2_1^+ \rightarrow 0_{\rm gs}^+$ transition ($E_\gamma =$ 658 keV) could be measured, exclusively. All other transitions ending at the ground state of ^{110}Cd were below the detection limit and considered negligible in the analysis. The total cross section for each beam energy was obtained in the same manner as previously. Final values of total cross sections and S factors are shown in Table II.

C. Theoretical calculations with TALYS

Theoretical calculations of the cross sections for the (p,γ) reactions have been carried out with the latest TALYS version (v1.8) [43], using various combinations of models for the three quantities considered by the Hauser-Feshbach model, i.e., OMP, NLD, and γSF. Several default options in TALYS have been tried for both reactions (corresponding to nearly 100 different combinations for each isotope) with a 5-keV energy step between 1.5 and 6 MeV. From the aggregated results, a region bounded by the maximum and minimum values at each energy value was formed, indicated as a shaded area in Fig. 4. The OMP is expected to have a dominant effect on the total cross section at low energies; therefore for the higher energies in this study, particular focus has been given to understanding the effect different NLD and γSF models have on the calculated cross sections.

TABLE II. Cross sections and S factors of the reaction ^{109}Ag$(p,\gamma)^{110}$Cd vs energy. Columns are as in Table I.

E_p(lab) (keV)	$E_{\rm eff}$(lab) (keV)	$E_{\rm eff}$(c.m.) (keV)	σ (μb)	S factor (10^7 MeV b)
4000	3989	3952	20.6(46)	0.12(3)
3500	3488	3456	7.2(24)	0.18(6)
2200	2184	2164	0.14(59)	1.6(67)

For the production of ^{108}Cd and ^{110}Cd, experimental data are compared to calculations with various γSF options coupled to the optical model proposed by Bauge, Delaroche, and Girod (BDG) [49] and nuclear level densities by either Hilaire *et al.* (THFBG) [50] or Ignatyuk *et al.* (GSM) [51] (see Table III). The global semimicroscopic OMP by BDG is based on the microscopic OMP by Jeukenne, Lejeune, and Mahaux [52], while the THFBG NLD is based on the Hartree-Fock-Bogoliubov model using the effective nucleon-nucleon interaction D1M Gogny and a temperature-dependent treatment, which provides a way to deal with the modifications of the structure properties with increasing excitation energy. The particular combinations seem to produce values relatively close to the experimental ones, as reported in the present work, and have been investigated more thoroughly by considering several options of γSF.

IV. DISCUSSION AND CONCLUSIONS

In the framework of the present work, an experimental attempt to study two radiative proton-capture reactions, i.e., ^{107}Ag$(p,\gamma)^{108}$Cd and ^{109}Ag$(p,\gamma)^{110}$Cd, was carried out. The experimental results for the total cross sections and the astrophysical S factors of the two reactions are summarized in Tables I and II. In Fig. 4, the experimental data are shown together with theoretical calculations using TALYS. These calculations correspond to combining four different γSF models with the microscopic BDG's OMP and Hilaire *et al.*'s [50] microscopic nuclear level densities (temperature-dependent Hartree-Fock-Bogolubov with Gogny's force) (combinations TALYS1–TALYS4). The γSF models combined with BDG + THFBG are the empirical model by Kopecky and Uhl [53] (TALYS1); two microscopic models, which describe the ground-state properties of the nucleus by Hartree-Fock (HFB) (TALYS2) or Hartree-Fock-BCS (HFBCS) (TALYS3) and the excitation modes by quasirandom-phase approximation (QRPA) [54]; and the model Gogny D1M HFB + QRPA [55], which uses the finite-range D1M Gogny force and a

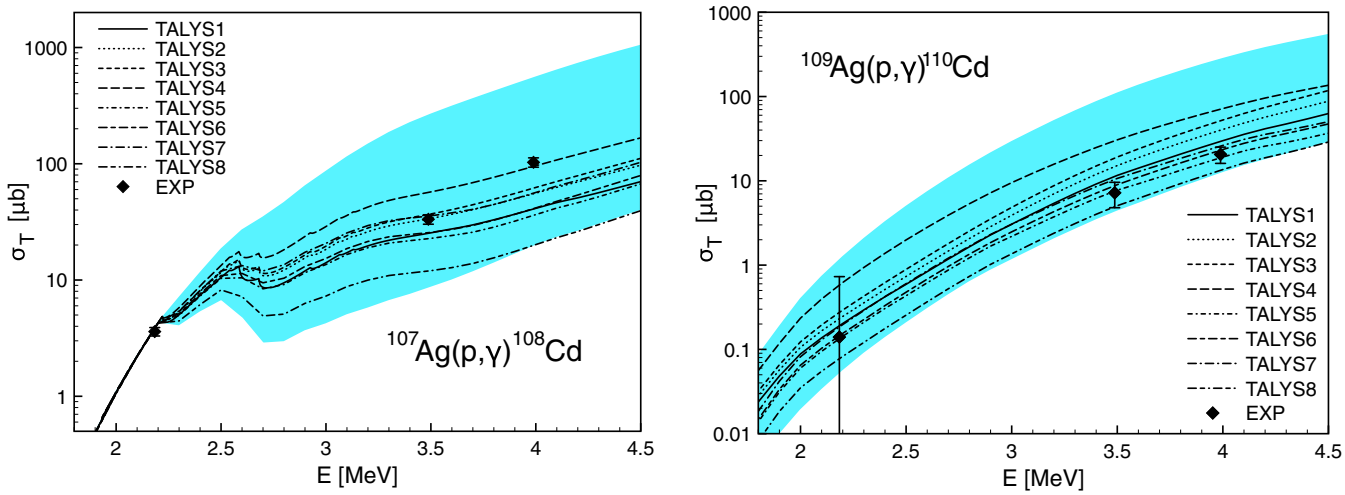

FIG. 4. Comparison between theoretical calculations with TALYS and experimentally deduced cross sections (in μb) for the reaction ^{107}Ag$(p,\gamma)^{108}$Cd (left panel) and the reaction ^{109}Ag$(p,\gamma)^{110}$Cd (right panel). Incident energy is expressed in the laboratory frame. See Table III for an explanation of the legend entries. Please note that y-axis scales are different in the plots. The shaded area is bounded by the maximum and minimum values found for each energy step during calculations.

folding of the QRPA strength by a normalized Lorentzian function (TALYS4). Further consideration was given to the combination of the BDG OMP with the GSM NLD [51] and four more options for the γSF (TALYS5–TALYS8). The GSM in its phenomenological option attributes its success to the inclusion of shell model, collective, and superfluid effects. The four employed γSF models are Kopecky-Uhl [53] (TALYS5); HFB [54] (TALYS6); the hybrid model by Goriely *et al.* [56], which unifies a low-energy description and a Lorentzian high-energy shape (TALYS7); and the self-consistent relativistic mean-field (RMF) model with the relativistic random phase approximation (RRPA) [56] (TALYS8). Table III summarizes all combinations mentioned above.

There is an overall good agreement between the data and the theoretical calculations. This holds even for the case of ^{109}Ag$(p,\gamma)^{110}$Cd despite the large uncertainties. The trend of experimental data is well reproduced by the theoretical calculations. Especially for ^{110}Cd, the TALYS1 combination (OMP: BDG; NLD: GSM; γSF: Kopecky-Uhl) seems to follow the data rather closely, both in trend and magnitude. It is necessary to stress that the existing large experimental uncertainties do not allow for a firm conclusion on which combination is the best choice. This is also true for the p nucleus ^{108}Cd, where no unique combination of models reproduces the experimental values very well. It should be mentioned that in TALYS4 there is consistency in the calculation of the NLD and the γSF with the use of Hartree-Fock-Bogolubov and the D1M Gogny effective interaction. Also, one can realize that at least in the case of ^{108}Cd there is almost no sensitivity in the NLD comparing the combinations TALYS1 and TALYS5, which use the γSF Kopecky-Uhl and THFBG and GSM as the NLDs, as well as the combinations TALYS2 and TALYS6, which use the γSF HFB tables and the two NLDs: THFBG and GSM. In any case, a full-scale sensitivity analysis is beyond the scope of this article and requires careful consideration of all possible models involved in the calculations, possibly by fine-tuning the input parameters incorporated in these models.

TABLE III. Combinations of models used for calculations with TALYS for the ^{107,109}Ag$(p,\gamma)^{108,110}$Cd reactions

Model	OMP	NLD	γSF
TALYS1	BDG[a]	THFBG[b]	Kopecky-Uhl [53]
TALYS2	BDG	THFBG	HFB tables [54]
TALYS3	BDG	THFBG	HFB-BCS tables [54]
TALYS4	BDG	THFBG	Gogny D1M HFB + QRPA [55]
TALYS5	BDG	GSM[c]	Kopecky-Uhl
TALYS6	BDG	GSM	HFB tables
TALYS7	BDG	GSM	Goriely's hybrid model [56]
TALYS8	BDG	GSM	RMF + RRPA [57]

[a]BDG: Bauge-Delaroche-Girod [49].
[b]THFBG: temperature-dependent HFB, Gogny force [50].
[c]GSM: generalized superfluid model [51].

For the reaction of protons with ^{107}Ag the competitive (p,n) channel has a known energy threshold at 2.219 MeV and several neutron resonances exist above this value. Below this threshold, all combinations converge rapidly onto each other, showing the expected indifference of the underlying mechanism to all quantities but the optical model potential. Such a threshold for the case of p + ^{109}Ag appears at a lower energy (1006.68 keV [48]) than the region of interest, as is also evident by the smoother curves illustrated in the right-hand panel of Fig. 4.

Theoretical calculations for the ^{107}Ag (p,n) ^{107}Cd reaction have been carried out simultaneously with the ones for the respective (p,γ) channel. The results are shown in Fig. 5. In the same figure, previous experimental (p,n) data by Hershberger *et al.* [19] have been included, and the agreement with the TALYS results is evident. It is worth-mentioning that the cross section of the reaction ^{107}Ag (p,n) ^{107}Cd for laboratory energies between 3 and 6 MeV has been evaluated in Ref. [19] by using a Hauser-Feshbach code (HELGA) and including the compound elastic channel. Its value is comparable to the one

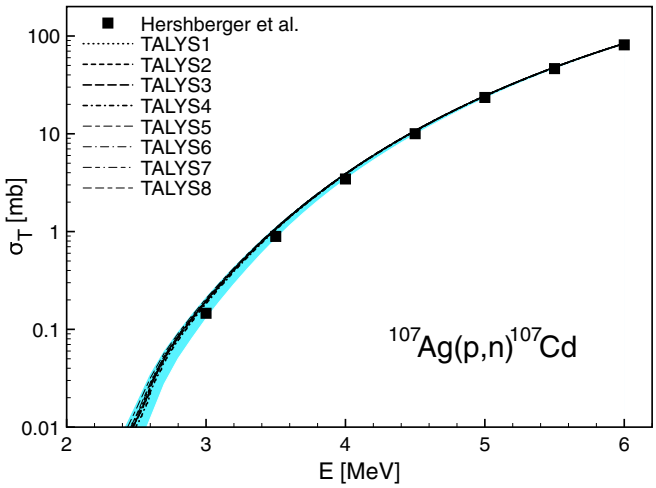

FIG. 5. The solid squares correspond to experimental cross sections (in mb) for the reaction ^{107}Ag (p,n) ^{107}Cd from Ref. [19]. The curves are TALYS1–TALYS8 output data produced simultaneously with the ones shown in the left-hand panel of Fig. 4 for the competing (p,γ) channel. The shaded area is as in Fig. 4.

for the ^{107}Ag (p,n) ^{107}Cd for laboratory energies around 3 MeV, but it gets smaller as the energy increases towards 6 MeV. Moreover, the extracted theoretical curves show good agreement with similar work on the (p,n) channel carried out for a more extended energy range by Leng *et al.* [58]. Among other things these researchers used various phenomenological OMPs to calculate cross sections for the (p,n) channel in a higher energy range (up to 340 MeV).

An important remark about the present analysis is the strong effect the choice of model combination has on the calculated cross sections. The roles of the NLD and γSF are pronounced at higher energies, while they become less important in lower energies as can be seen clearly in the case of the ^{108}Cd production. It is perhaps redundant to claim that further investigation is required for the nuclei examined here to provide firm evidence on specific mechanisms driving these processes, both at an experimental and a theoretical level. However, the underproduction of p nuclei in this mass region is a persistent motivation to continue researching, especially when the scarcity of data, even for stable nuclei, is considered.

It is generally accepted that with this particular technique some weak transitions may be absent from the spectra, resulting in missing strengths. Such cases require further investigation with complementary techniques. The present results provide new information on the intriguing and relatively unexplored p process. Contributing to future endeavors, these measurements in this work offer an important starting point in understanding the nuclear parameters defining dynamic astrophysical environments, serving at the same time as benchmark values for theoretical modeling and future experimental works.

ACKNOWLEDGMENTS

We are thankful to the staff of the "Demokritos" Tandem Accelerator Lab for their assistance during the experiment. T.J.M. is indebted to Dr. S. Harissopulos and Professor A. Spyrou for useful discussions.

[1] E. M. Burbidge, G. R. Burbidge, W. A. Fowler, and F. Hoyle, Rev. Mod. Phys. **29**, 547 (1957).
[2] A. G. W. Cameron, Publ. Astron. Soc. Pac. **69**, 201 (1957).
[3] I. Dillmann, T. Szücs, R. Plag, Z. Fülöp, F. Käppeler, A. Mengoni, and T. Rauscher, Nucl. Data Sheets **120**, 171 (2014).
[4] M. Arnould and S. Goriely, Phys. Rep. **384**, 1 (2003).
[5] T. Rauscher, N. Dauphas, I. Dillmann, C. Fröhlich, Z. Fülöp, and G. Gyürky, Rep. Prog. Phys. **76**, 066201 (2013).
[6] H. Palme and A. Jones, in *Treatise on Geochemistry*, edited by H. D. H. K. Turekian (Pergamon, Oxford, 2003), pp. 41–61.
[7] K. Lodders, Solar system abundances of the elements, in *Principles and Perspectives in Cosmochemistry: Lecture Notes of the Kodai School on 'Synthesis of Elements in Stars' held at Kodaikanal Observatory, India, April 29–May 13, 2008*, edited by A. Goswami and B. E. Reddy (Springer, Berlin, 2010), pp. 379–417.
[8] J. Audouze and J. W. Truran, Astrophys. J. **202**, 204 (1975).
[9] S. E. Woosley and W. M. Howard, Astrophys. J. Suppl. **36**, 285 (1978).
[10] M. Rayet, M. Arnould, M. Hashimoto, N. Prantzos, and K. Nomoto, Astron. Astrophys. **298**, 517 (1995).
[11] T. Rauscher, A. Heger, R. D. Hoffman, and S. E. Woosley, Astrophys. J. **576**, 323 (2002).
[12] W. Rapp, J. Görres, M. Wiescher, H. Schatz, and F. Käppeler, Astrophys. J. **653**, 474 (2006).
[13] C. Travaglio, F. K. Röpke, R. Gallino, and W. Hillebrandt, Astrophys. J. **739**, 93 (2011).
[14] H. Schatz, A. Aprahamian, J. Görres, M. Wiescher, T. Rauscher, J. Rembges, F.-K. Thielemann, B. Pfeiffer, P. Möller, K.-L. Kratz, H. Herndl, B. Brown, and H. Rebel, Phys. Rep. **294**, 167 (1998).
[15] H. Schatz, A. Aprahamian, V. Barnard, L. Bildsten, A. Cumming, M. Ouellette, T. Rauscher, F.-K. Thielemann, and M. Wiescher, Phys. Rev. Lett. **86**, 3471 (2001).
[16] S. Goriely, J. José, M. Hernanz, M. Rayet, and M. Arnould, Astron. Astrophys. **383**, L27 (2002).
[17] C. Fröhlich, G. Martínez-Pinedo, M. Liebendörfer, F.-K. Thielemann, E. Bravo, W. R. Hix, K. Langanke, and N. T. Zinner, Phys. Rev. Lett. **96**, 142502 (2006).
[18] J. Batchelder, T. Kawano, J. Kelley, F. G. Kondev, E. McCutchan, M. Smith, A. Sonzogni, M. Thoennessen, and I. Thompson, White Paper on Nuclear Data Needs and Capabilities for Basic Science, Lawrence Livermore National Laboratory, Report No. LLNL-TR-731502 (2017).
[19] R. L. Hershberger, D. S. Flynn, F. Gabbard, and C. H. Johnson, Phys. Rev. C **21**, 896 (1980).
[20] C. H. Johnson, A. Galonsky, and R. L. Kernell, Phys. Rev. C **20**, 2052 (1979).
[21] M. U. Khandaker, K. Kim, K.-S. Kim, M. Lee, G. Kim, Y. S. Cho, and Y. O. Lee, Nucl. Instrum. Methods Phys. Res., Sect. B **266**, 5101 (2008).
[22] S. Harissopulos, E. Skreti, P. Tsagari, G. Souliotis, P. Demetriou, T. Paradellis, J. W. Hammer, R. Kunz, C. Angulo, S. Goriely, and T. Rauscher, Phys. Rev. C **64**, 055804 (2001).

[23] S. Galanopoulos, P. Demetriou, M. Kokkoris, S. Harissopulos, R. Kunz, M. Fey, J. W. Hammer, G. Gyürky, Z. Fülöp, E. Somorjai, and S. Goriely, Phys. Rev. C **67**, 015801 (2003).
[24] A. Sauerwein, J. Endres, L. Netterdon, A. Zilges, V. Foteinou, G. Provatas, T. Konstantinopoulos, M. Axiotis, S. F. Ashley, S. Harissopulos, and T. Rauscher, Phys. Rev. C **86**, 035802 (2012).
[25] S. Harissopulos, A. Spyrou, A. Lagoyannis, M. Axiotis, P. Demetriou, J. W. Hammer, R. Kunz, and H.-W. Becker, Phys. Rev. C **87**, 025806 (2013).
[26] L. Netterdon, J. Mayer, P. Scholz, and A. Zilges, Phys. Rev. C **91**, 035801 (2015).
[27] S. Harissopulos, A. Spyrou, V. Foteinou, M. Axiotis, G. Provatas, and P. Demetriou, Phys. Rev. C **93**, 025804 (2016).
[28] C. Yalçin, R. T. Güray, N. Özkan, S. Kutlu, G. Gyürky, J. Farkas, G. G. Kiss, Z. Fülöp, A. Simon, E. Somorjai, and T. Rauscher, Phys. Rev. C **79**, 065801 (2009).
[29] G. Kiss, T. Rauscher, T. Szücs, Z. Kertész, Z. Fülöp, G. Gyürky, C. Fröhlich, J. Farkas, Z. Elekes, and E. Somorjai, Phys. Lett. B **695**, 419 (2011).
[30] I. Dillmann, L. Coquard, C. Domingo-Pardo, F. Käppeler, J. Marganiec, E. Uberseder, U. Giesen, A. Heiske, G. Feinberg, D. Hentschel, S. Hilpp, H. Leiste, T. Rauscher, and F.-K. Thielemann, Phys. Rev. C **84**, 015802 (2011).
[31] A. Sauerwein, H.-W. Becker, H. Dombrowski, M. Elvers, J. Endres, U. Giesen, J. Hasper, A. Hennig, L. Netterdon, T. Rauscher, D. Rogalla, K. O. Zell, and A. Zilges, Phys. Rev. C **84**, 045808 (2011).
[32] Z. Halász, G. Gyürky, J. Farkas, Z. Fülöp, T. Szücs, E. Somorjai, and T. Rauscher, Phys. Rev. C **85**, 025804 (2012).
[33] L. Netterdon, P. Demetriou, J. Endres, U. Giesen, G. Kiss, A. Sauerwein, T. Szücs, K. Zell, and A. Zilges, Nucl. Phys. A **916**, 149 (2013).
[34] L. Netterdon, A. Endres, G. G. Kiss, J. Mayer, T. Rauscher, P. Scholz, K. Sonnabend, Z. Török, and A. Zilges, Phys. Rev. C **90**, 035806 (2014).
[35] R. T. Güray, N. Özkan, C. Yalçin, T. Rauscher, G. Gyürky, J. Farkas, Z. Fülöp, Z. Halász, and E. Somorjai, Phys. Rev. C **91**, 055809 (2015).
[36] N. Kinoshita, K. Hayashi, S. Ueno, Y. Yatsu, A. Yokoyama, and N. Takahashi, Phys. Rev. C **93**, 025801 (2016).
[37] A. Spyrou, H.-W. Becker, A. Lagoyannis, S. Harissopulos, and C. Rolfs, Phys. Rev. C **76**, 015802 (2007).
[38] A. Spyrou, A. Lagoyannis, P. Demetriou, S. Harissopulos, and H.-W. Becker, Phys. Rev. C **77**, 065801 (2008).
[39] A. Spyrou *et al.*, Phys. Rev. C **88**, 045802 (2013).
[40] F. Naqvi, S. J. Quinn, A. Spyrou, A. Battaglia, M. Couder, P. A. DeYoung, A. C. Dombos, X. Fang, J. Görres, A. Kontos, Q. Li, S. Lyons, D. Robertson, A. Simon, K. Smith, M. K. Smith, E. Stech, W. P. Tan, and M. Wiescher, Phys. Rev. C **92**, 025804 (2015).
[41] B. Mei *et al.*, Phys. Rev. C **92**, 035803 (2015).
[42] W. Hauser and H. Feshbach, Phys. Rev. **87**, 366 (1952).
[43] A. Koning, S. Hilaire, and S. Goriely, TALYS-1.8, A Nuclear Reaction Program, NRG-1755 ZG Petten, The Netherlands (2015).
[44] K. J. R. Rosman and P. D. P Taylor, Pure Appl. Chem. **70**, 217 (1998).
[45] P. Tsavalas (private communication).
[46] J. R. T. M. Nastasi, *Handbook of Modern Ion Beam Materials Analysis* (Materials Research Society, Pittsburgh, 1995).
[47] J. F. Ziegler, M. D. Ziegler, and J. P. Biersack, Nucl. Instrum. Methods Phys. Res., Sect. B **268**, 1818 (2010).
[48] The Evaluated Nuclear Structure Data File (ENDSF), http://www.nndc.bnl.gov/endsf/.
[49] E. Bauge, J. P. Delaroche, and M. Girod, Phys. Rev. C **63**, 024607 (2001).
[50] S. Hilaire, M. Girod, S. Goriely, and A. J. Koning, Phys. Rev. C **86**, 064317 (2012).
[51] A. V. Ignatyuk, J. L. Weil, S. Raman, and S. Kahane, Phys. Rev. C **47**, 1504 (1993).
[52] J.-P. Jeukenne, A. Lejeune, and C. Mahaux, Phys. Rev. C **16**, 80 (1977).
[53] J. Kopecky and M. Uhl, Phys. Rev. C **41**, 1941 (1990).
[54] R. Capote *et al.*, Nucl. Data Sheets **110**, 3107 (2009), Special Issue on Nuclear Reaction Data.
[55] M. Martini, S. Hilaire, S. Goriely, A. Koning, and S. Péru, Nucl. Data Sheets **118**, 273 (2014).
[56] S. Goriely, Phys. Lett. B **436**, 10 (1998).
[57] D. Pena Arteaga and P. Ring, Phys. Rev. C **77**, 034317 (2008).
[58] Z.-p. Leng, K.-q. Zhang, and Z.-j. Zhang, At. Energy Sci. Technol. **47**, 705 (2013).